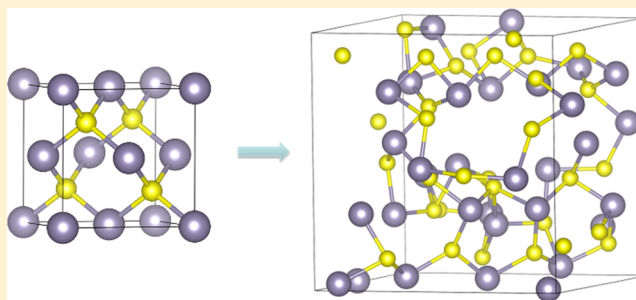


Phase Stability of the Earth-Abundant Tin Sulfides SnS, SnS₂, and Sn₂S₃

Lee A. Burton and Aron Walsh*

Centre for Sustainable Chemical Technologies, Department of Chemistry, University of Bath, Bath, U.K.

ABSTRACT: The various phases of tin sulfide have been studied as semiconductors since the 1960s and are now being investigated as potential earth-abundant photovoltaic and photocatalytic materials. Of particular note is the recent isolation of zincblende SnS in particles and thin-films. Herein, first-principles calculations are employed to better understand this novel geometry and its place within the tin sulfide multiphasic system. We report the enthalpies of formation for the known phases of SnS, SnS₂, and Sn₂S₃, with good agreement between theory and experiment for the ground-state structures of each. While theoretical X-ray diffraction patterns do agree with the assignment of the zincblende phase demonstrated in the literature, the structure is not stable close to the lattice parameters observed experimentally, exhibiting an unfeasibly large pressure and a formation enthalpy much higher than any other phase. Ab initio molecular dynamics simulations reveal spontaneous degradation to an amorphous phase much lower in energy, as Sn(II) is inherently unstable in a regular tetrahedral environment. We conclude that the known rocksalt phase of SnS has been mis-assigned as zincblende in the recent literature.



INTRODUCTION

Photovoltaic (PV) devices are of growing importance due to increasing population and diminishing reserves. Today, PV technology predominantly uses silicon as an absorber material but because of the low optical absorption coefficient, up to 500 μm thick films are needed to absorb significant fractions of visible light. More optimal absorber materials need less than 5 μm thickness,¹ giving rise to so-called thin-film technologies that require less material and much cheaper processing conditions than silicon, indeed the lowest among commercial PV technologies.² Successful examples include the commercially available cadmium telluride (CdTe) and copper–indium–gallium–selenide (CIGS) cells that have achieved record efficiencies close to 20%.³ Unfortunately, tellurium, indium, and gallium are rare and expensive; alternatives must be sought if PV is ever to scale up to the level of energy generation provided by nonrenewable methods: tera-watt production.

Quaternary blends of more common elements can circumvent the issue of precursor availability and cost; where properties are tailored to PV applications by varying the stoichiometry of individual components.⁴ Most notable among these is Cu₂ZnSnS₄ (CZTS), which has achieved efficiencies of greater than 10%.⁵ As an alloy of Cu₂S, ZnS, and SnS₂, element availability is not a concern, but controlling the component ratios can be difficult. It has been shown that the desirable phase of CZTS occupies just a small fraction of the overall phase space for the system^{6,7} and has little or no thermodynamic barrier to phase separation.⁸

Herein, we consider tin sulfide, which is one of the components of CZTS and is itself attractive for PV applications because it is abundant, environmentally benign, and inex-

pensive.⁹ For example, tin extraction and importation to the European Union has an associated carbon footprint of less than one tenth of that of gallium (data obtained from “tin at regional storage” system process and “gallium, semiconductor grade, at regional storage” system process of theecoinvent database within SimaPro7 software) and has an occurrence of 2 ppm on the earth’s crust.¹⁰

Tin sulfide single crystals have been grown by the Bridgman method and chemical vapor transport;^{11,12} and thin-films can be formed by chemical vapor deposition,¹³ chemical bath deposition,¹⁴ atomic layer deposition,¹⁵ electrodeposition,¹⁶ sulfurization of tin films,¹⁷ solid-state multilayer synthesis,¹⁸ and successive ionic layer adsorption and reaction.¹⁹ Nanostructures reported to date include, but are not limited to, nanoporous SnS frameworks by templated synthesis,²⁰ nanodisks by electrodeposition,²¹ nanosheets by pyrolysis,²² nanoflowers by hydrothermal synthesis,²³ nanobelts by a molten salt solvent method,²⁴ and fullerene-like nanoparticles by laser ablation.²⁵

Significantly, it has been claimed that zincblende (ZB) tin monosulfide microparticles have been synthesized²⁶ and deposited as thin-films.¹⁰ This would allow for increased compatibility with existing technologies based on II–VI and III–V tetrahedral semiconductors. For example, the current generation of thin-film solar cells relies on a clean interface between the absorber material and the zincblende structured cadmium sulfide window layer. ZB structures also tend to exhibit a direct fundamental bandgap and large optical

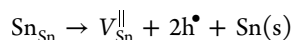
Received: September 14, 2012

Revised: October 24, 2012

Published: November 5, 2012

absorption coefficients, which could serve to increase tin sulfide's performance as a PV material.

Most work agrees that orthorhombic SnS has a direct optical bandgap of 1.30–1.43 eV,^{27–29} while older work³⁰ and a recent theoretical study advocate an indirect bandgap at 1.07 eV.³¹ Regardless, all investigations agree on an effective optical absorption onset around 1.4 eV, which coincides with the optimum band gap for maximum efficiency according to the Shockley–Queisser limit within the AM 1.5 solar spectrum.³² SnS also has a higher optical absorption coefficient than CdTe and other existing PV materials,^{27,33} with intrinsic p-type conductivity considered to be brought about by the formation of tin vacancies according to the defect reaction:³⁴



The ease of forming these vacancies is a potential source of discrepancy between reported properties and why, despite being an ideal candidate for PV applications, SnS devices have not yet surpassed 1.3% efficiency.²⁷

In this article, we report the enthalpies of formation of the known phases of the tin sulfides and compare the relative stability of each. The values are calculated using a first-principles electronic structure method based on density functional theory. While good agreement is found between theory and the known ground-state phases, there are deviations between the expected properties of zincblende SnS and those obtained using the level of theory employed in this work, calling into question the validity of recent experimental assignments. Indeed, the known rocksalt (RS) phase of SnS gives rise to the same powder diffraction pattern, with a cubic lattice constant similar to that identified for the ZB phase, which leads us to conclude that the latter structures have been incorrectly assigned in recent experiments.

COMPUTATIONAL METHODS

The unique crystal structures of all tin sulfide phases were identified from the inorganic crystal structure database (ICSD). Density functional theory (DFT) as implemented in the Fritz Haber Institut ab initio molecular simulations (FHI-AIMS) package was used to calculate the equilibrium geometry and total energy for each structure.^{35–37} To describe the effect of electron exchange and correlation, the semilocal generalized gradient approximation (GGA) was applied within the density functional of Perdew, Burke, and Ernzerhof optimized for solids (PBEsol).³⁸ Local numerical orbital basis sets were used along with periodic boundary conditions applied in 3 dimensions to approximate bulk solids. A well-converged Tier-2 basis set was employed for each species, with scalar-relativistic effects treated at the scaled ZORA level of theory.³⁹ Finally, the k -point density was checked for convergence to within 0.01 eV per formula unit.

All calculations were performed in closed shell configuration (restricted spin), with geometry relaxations undertaken using the Broyden–Fletcher–Goldfarb–Shanno (BFGS) algorithm and a force convergence criterion tolerance in all cases of 0.01 eV/Å.⁴⁰

In order to assess dynamic phase stability, ab initio molecular dynamics (MD) simulations were carried out within the Nose–Hoover thermostat of the NVT canonical ensemble. This approach combines DFT forces with classical Newtonian mechanics, and a time-step of 1 fs. The temperature ranges modeled were 300, 500, 700, and 1000 K. The systems were

brought to equilibrium over 5 ps and quenched directly to 0 K, followed by the standard local optimization procedure.

RESULTS

Crystal Structures. SnS preferentially crystallizes in the orthorhombic herzenbergite structure, with the space group $Pnma$. In this structure, the Sn^{2+} ion coordinates to three S^{2-} ions, with the Sn $5s^2$ lone pair occupying the last position of a tetrahedral geometry, following the revised lone pair model.⁴¹ Other phases of SnS that are of interest are the rocksalt structure grown under epitaxial strain,⁴² the high temperature orthorhombic structure,⁴³ and the ZB structure first reported in 1962 from SnS evaporation onto rocksalt,⁴⁴ with further reports occurring only very recently.^{10,26}

The different SnS geometries are shown in Figure 1 along with the ground-state structures of SnS_2 and Sn_2S_3 . The low

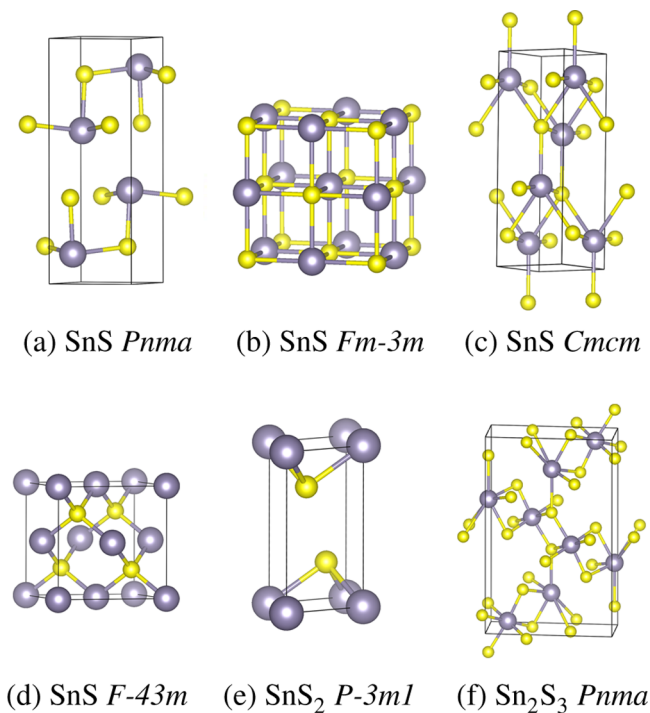


Figure 1. Crystal structures of tin (gray) monosulfide (yellow) and the ground-state structures of SnS_2 and Sn_2S_3 .

energy phase of SnS_2 is a hexagonal structure composed of SnS_2 trilayers, where the Sn(IV) ion is coordinated to six S ions in an octahedral environment, which is similar, for example, to that found in rutile-structured SnO_2 . Alternate stacking of the trilayers results in a series of structural polytypes, as typified by the isostructural CdI_2 system.

The crystal structure of tin sesquisulfide is tetragonal and shares the same space group as the ground-state phase of SnS. The structure is composed of Sn_2S_3 chains, with the Sn(IV) ions adopting chain-center positions with octahedral coordination to S, and the Sn(II) ions adopting chain-end positions in the favored trigonal-pyramidal arrangement. Hence, the coordination preferences of both Sn oxidation states can be simultaneously satisfied. The space group labels for SnS correspond to the following structures: $Pnma$, the orthorhombic ground-state phase; $Fm\bar{3}m$, the rocksalt phase; $Cmcm$, the orthorhombic, high temperature phase; and $F\bar{4}3m$, the zincblende phase.

Table 1. Reported Structural Parameters from X-ray Diffraction Measurements and Geometries Relaxed within PBEsol-DFT

phase	space group	experimental parameters			ref	relaxed parameters (% error)		
		<i>a</i>	<i>b</i>	<i>c</i>		<i>a</i>	<i>b</i>	<i>c</i>
SnS	<i>Pnma</i>	11.32	4.05	4.24	43	11.11 (1.89)	3.99 (1.52)	4.24 (0.10)
SnS	<i>Fm$\bar{3}m$</i>	5.8	5.8	5.8	45	5.75 (0.87)	5.75 (0.87)	5.75 (0.87)
SnS	<i>F$\bar{4}3m$</i>	5.845	5.845	5.845	26	6.43 (10.0)	6.43 (10.0)	6.43 (10.0)
SnS ₂	<i>P$\bar{3}m1$</i>	3.64	3.64	5.89	46	3.66 (0.44)	3.67 (0.80)	6.06 (2.75)
Sn ₂ S ₃	<i>Pnma</i>	8.87	3.75	14.02	12	8.80 (0.83)	3.77 (0.66)	13.83 (1.36)
SnO	<i>P4/n m m</i>	3.80	3.80	4.82	47	3.81 (0.26)	3.81 (0.26)	4.76 (1.09)
SnO ₂	<i>P42/mmm</i>	4.74	4.74	3.19	48	4.77 (0.72)	4.77 (0.72)	3.22 (0.97)

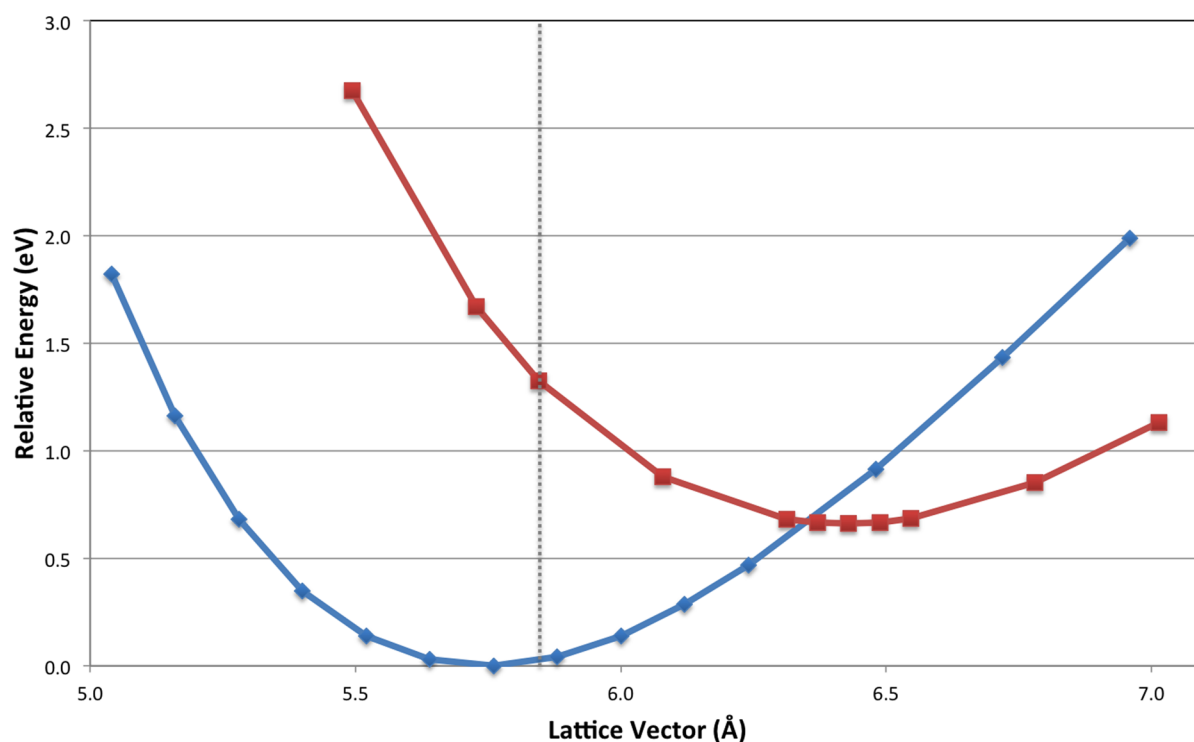


Figure 2. Energy–volume curve for zincblende (red) and rocksalt (blue) SnS. The reported lattice parameter of 5.845 Å is indicated with a vertical line and the energy is plotted per SnS.²⁶

Table 1 contains the lattice parameters for the different SnS phases. For the ground-state structures, the calculated lattice parameters are in excellent agreement with experiment, where the error is typically less than 2%. One exception is the *c* axis of SnS₂, which is overestimated to 2.75% due to the nonbonding nature of the interlayer interactions (van der Waals interactions are not well described at this level of theory). The *Cmcm* phase could not be stabilized as it undergoes a second-order phase transition to the ground-state *Pnma* structure, which is observed experimentally at 878 K.⁴⁹ A significant discrepancy is only observed between the calculated and measured lattice parameters for the ZB *F $\bar{4}3m$* structure.

The equilibrium lattice parameter of the ZB phase is 10% larger than the reported value. This has been checked with other DFT functionals (local, semilocal, and nonlocal variants) and implementations (i.e., the VASP code).⁵⁰ The calculated energy–volume curve is shown in Figure 2 alongside that of the rocksalt (*Fm $\bar{3}m$*) phase. The slope of the curves represents the effective pressure of the system, i.e. $P = -(\partial U/\partial V)_T$, which for the observed ZB lattice parameter corresponds to an extremely large pressure of around 930 GPa, and can clearly not be representative of an equilibrium state. On the other hand, we

direct the readers attention to the similarity between the experimental ZB lattice parameter and the equilibrium rocksalt lattice parameter.

The dynamic instability of the ZB phase was confirmed by a spontaneous distortion in MD simulations at room temperature (300 K), as well as the presence of large imaginary frequencies in phonon calculations. Three plausible explanations exist for this behavior: (i) the actual phase found in experiment is not ZB; (ii) the phase is formed in a highly strained environment; and (iii) the phase is stabilized by a high concentration of lattice defects. However, the large size of the particles reported by Greyson et al.²⁶ leads us to conclude that explanation (i) is most likely.

Enthalpies of Formation. Enthalpies of formation are key to understanding the relative stabilities of a multiphase system as they indicate which conformation the system would preferentially adopt. Indeed, simple thermodynamic arguments have been shown to play a fundamental role in the design, optimization, and performance of solar cell devices due to issues associated with phase mixing and separation across interfaces.⁵¹ The following results, obtained from PBEsol-DFT calculations, formally represent values at 0 K and do not

account for any prohibitive kinetic barriers involved in structural change. We define the enthalpies according to the reaction $x\text{Sn}(s) + y\text{S}(s) \rightarrow \text{Sn}_x\text{S}_y$.

The enthalpies of formation for tin monosulfide shown in Table 2 agree very well with experiment, whereas the formation

Table 2. Enthalpies of Formation Calculated in This Work and Compared to Experimental Data Where Available

phase	space group	ΔH_f^{DFT} (in eV and kJ mol^{-1})		ΔH_f^{exp} (kJ mol^{-1})
SnS	<i>Pnma</i>	-1.03	-99.35	-100 to -108 ^{52,53}
SnS	<i>Fm$\bar{3}m$</i>	-0.95	-91.66	
SnS	<i>F$\bar{4}3m$</i>	-0.29	-27.80	
SnS ₂	<i>P$\bar{3}m1$</i>	-1.36	-130.99	-148 to -182 ⁵³⁻⁵⁵
Sn ₂ S ₃	<i>Pnma</i>	-2.39	-230.35	-249 to -297 ⁵³⁻⁵⁵

enthalpies for SnS₂ and Sn₂S₃ deviate significantly. In the opinion of the authors, this result reflects more on the difficulty of obtaining phase pure materials experimentally than on the accuracy of the level of theory employed in this work, which is supported by the large variation in the measured enthalpies of formation.

The calculated enthalpy of formation for individual phases plotted against elemental composition affords a convenient method of comparing phase stabilities for any binary state. A convex hull is a plot of this kind, with the lowest energy states connected to form the base of a hull and any higher energy states appearing above this line, is shown in Figure 3. The convex hull also indicates the energies of alternate composition ratios for that system.

Together with the results described in Table 2, the convex hull for the tin sulfides shows that ZB (*F $\bar{4}3m$*) tin monosulfide should not be thermodynamically accessible under normal synthesis conditions; it lies 0.74 eV above the ground state *Pnma* phase. Considering that *Cmcm* SnS does not form below

$878 \pm 5 \text{ K}$,⁴⁹ it is possible to see the relative magnitude of internal energy inherent to ZB SnS. The energy of the ZB phase is associated with the optimized lattice parameters reported in Table 1. Even higher energies are obtained for the ZB structure using experimental lattice constants, with the difference between them shown in Figure 2. In contrast, rocksalt SnS, while not the ground-state, should still be thermodynamically accessible.

Predicted X-ray Diffraction Patterns. The predicted X-ray diffraction patterns for rocksalt and zincblende SnS, at the same lattice spacing, are shown in Figure 4. One can see that the peak positions and the reflections associated with each are equivalent, due to the common fcc crystal structure, and it would be possible to confuse the two. We cannot account for the preferential orientation of crystals due to the dependence of the growth process on nucleation,⁵⁶ but a powder diffraction of each would show that ZB SnS exhibits a stronger (111) reflection at $2\theta = 26.8^\circ$, whereas rocksalt SnS would have a stronger (002) reflection at $2\theta = 31.0$. In previous work, the intensity ratios predicted for ZB SnS were not adhered to in ascribing the ZB structure from the diffraction pattern, and this could be important in distinguishing between the two phases.¹⁰ Both of these patterns correspond exactly with the peak positions of the XRD of ZB SnS reported by both Greyson et al. and Avellaneda et al. for nanoparticulate and thin-film tin sulfides, respectively.^{10,26}

DISCUSSION

Our calculations show good agreement with observed crystal parameter values for the majority of the tin sulfide family of compounds, with the main outstanding issue being relating to the cubic zincblende phase of SnS.

The ZB monosulfide appears unusually high in energy and spontaneously distorts when allowed to relax even at room temperature. Quenching of the ZB (a $2 \times 2 \times 2$ 64-atom

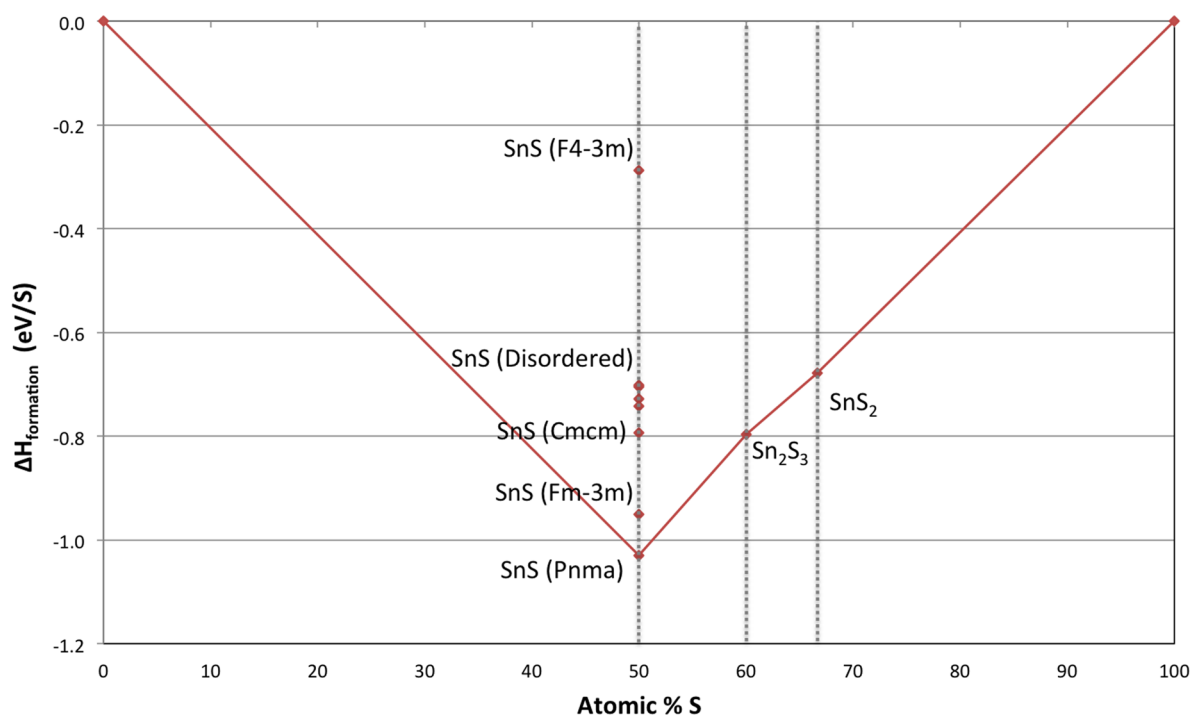


Figure 3. Convex hull showing enthalpy of formation against atomic percent of sulfur present in each phase.

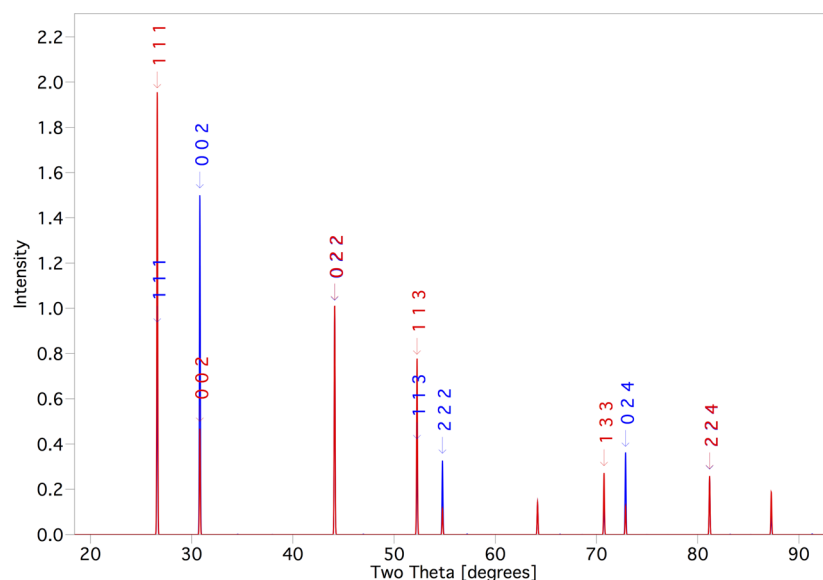


Figure 4. Predicted X-ray diffraction spectra for rocksalt (blue) and zincblende (red) SnS.

supercell) structure from temperatures of 300–1000 K resulted in a series of disordered phases, one of which is shown in Figure 5. The distribution in energy of these amorphous

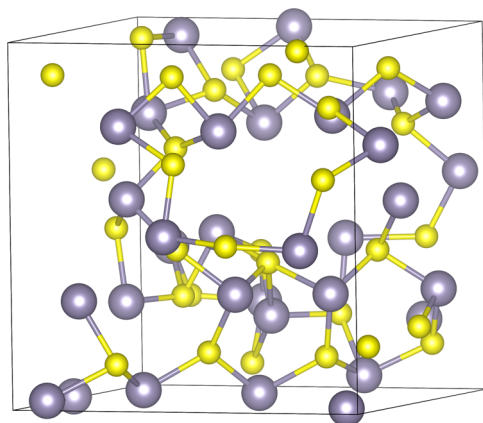


Figure 5. Structure of a typical amorphous SnS obtained upon quenching an MD simulation of the ZB phase.

structures is included in Figure 3. The amorphous structures all have energies more than 0.4 eV lower than ZB itself and contain predominantly 3-fold coordinate tin in a trigonal-pyramidal geometry. This is the typically adopted conformation of the ground-state tin sulfide structures, and one can see the orientation of the stereochemically active lone pairs on tin toward cavities in the lattice, as found for other tin compounds.^{57,58}

It has been shown that the formation of an asymmetric electron density on Sn(II) is induced by a tetrahedral environment with sulfur, due to orbital interactions (Sn 5s–5p hybridization).⁵⁹ The same interaction is prohibited by the inversion symmetry of rocksalt,⁶⁰ lending further credence to the phase instabilities reported in this work. It should be noted that the tetrahedral geometry is known and stable for the Sn(IV) oxidation state, where the valence electronic configuration is 5s⁰5p⁰, i.e., the s orbitals are formally empty. Examples range from molecular SnCl₄ to metal sulfides such as CZTS and metal phosphides such as ZnSnP₂.⁶¹

Finally, the predicted diffraction patterns shown in this work highlight a possible source of confusion in the recent studies of tin sulfide. We propose that the known rocksalt phase has been mis-assigned as zincblende.

CONCLUSIONS

In conclusion, we have assessed the structural and thermodynamic properties of SnS, SnS₂, and Sn₂S₃ from first-principles calculations. Good agreement with experiment is obtained, with the exception of zincblende SnS, which is predicted to be thermodynamically and dynamically unstable. The predictions match the expectation from textbook inorganic chemistry that high-symmetry coordination environments are adopted by the Sn(IV) ion, but the Sn(II) ion favors asymmetric environments of low coordination. A spontaneous distortion from tetrahedral to trigonal-pyramidal arrangement is observed to occur. Recent experimental reports could be explained by (i) a structural misassignment; (ii) highly strained crystallites; and (iii) high concentrations of lattice defects forming a superlattice structure. However, on the basis of the equivalent nature of reflections in the RS and ZB diffraction patterns, we propose that the known rocksalt phase of SnS has been mis-assigned as zincblende in recent reports.

AUTHOR INFORMATION

Corresponding Author

*E-mail: a.walsh@bath.ac.uk.

Notes

The authors declare no competing financial interest.

ACKNOWLEDGMENTS

We thank Kieran Molloy, Chris Bowen, and Laurie Peter (Bath) for useful discussions and Gilles Dennler (IMRA-Europe) for suggesting the topic. A.W. acknowledges support from the Royal Society University Research Fellowship scheme, and L.B. is funded by EPSRC (Grant No. EP/G03768X/1). Access to the HECToR supercomputer was facilitated through membership of the HPC Materials Chemistry Consortium, which is funded by EPSRC (Grant No. EP/F067496). Images of chemical structure were made using VESTA software.⁶²

REFERENCES

- (1) Nelson, J. *The Physics of Solar Cells*; Imperial College Press: London, 2003.
- (2) Fthenakis, V. *Renewable Sustainable Energy Rev.* **2009**, *13*, 2746–2750.
- (3) Green, M. A.; Emery, K.; Hishikawa, Y.; Warta, W. *Prog. Photovoltaics Res. Appl.* **2011**, *19*, 84–92.
- (4) Chen, S.; Gong, X. G.; Walsh, A.; Wei, S. H. *Phys. Rev. B* **2009**, *79*, 165211.
- (5) Bag, S.; Gunawan, O.; Gokmen, T.; Zhu, Y.; Todorov, T. K.; Mitzi, D. B. *Energy Environ. Sci.* **2012**, *5*, 7060–7065.
- (6) Chen, S.; Gong, X. G.; Walsh, A.; Wei, S. H. *Appl. Phys. Lett.* **2010**, *96*, 021902–3.
- (7) Chen, S.; Yang, J. H.; Gong, X. G.; Walsh, A.; Wei, S. H. *Phys. Rev. B* **2010**, *81*, 245204.
- (8) Zhai, Y. T.; Chen, S.; Yang, J. H.; Xiang, H. J.; Gong, X. G.; Walsh, A.; Kang, J.; Wei, S. H. *Phys. Rev. B* **2011**, *84*, 075213.
- (9) Peter, L. M. *Philos. Trans. R. Soc. London, Ser. A* **2011**, *369*, 1840–1856.
- (10) Avellaneda, D.; Nair, M. T. S.; Nair, P. K. J. *Electrochem. Soc.* **2008**, *155*, D517–D525.
- (11) Vyas, S. M.; Pandya, G. R.; Desai, C. F. *Indian J. Pure. Appl. Phys.* **1995**, *33*, 191–194.
- (12) Cruz, M.; Morales, J.; Espinos, J. P.; Sanz, J. J. *Solid State Chem.* **2003**, *175*, 359–365.
- (13) Kana, A. T.; Hibbert, T. G.; Mahon, M. F.; Molloy, K. C.; Parkin, I. P.; Price, L. S. *Polyhedron* **2001**, *20*, 2989–2995.
- (14) Nair, P. K.; Nair, M. T. S.; Garcia, V. M.; Arenas, O. L.; Pena, Y.; Castillo, A.; Ayala, I. T.; Gomezdaza, O.; Sanchez, A.; Campos, J.; Hu, H.; Suarez, R.; Rincon, M. E. *Sol. Energy Mater. Sol. Cells* **1998**, *52*, 313–344.
- (15) Kim, J. Y.; George, S. M. *J. Phys. Chem. C* **2010**, *114*, 17597–17603.
- (16) Ghazali, A.; Zainal, Z.; Hussein, M. Z.; Kassim, A. *Sol. Energy Mater. Sol. Cells* **1998**, *55*, 237–249.
- (17) Sugiyama, M.; Miyauchi, K.; Minemura, T.; Ohtsuka, K.; Noguchi, K.; Nakanishi, H. *Jpn. J. Appl. Phys.* **2008**, *47*, 4494–4495.
- (18) Xu, Z.; Chen, Y. *Semicond. Sci. Technol.* **2012**, *27*, 035007.
- (19) Ghosh, B.; Das, M.; Banerjee, P.; Das, S. *Appl. Surf. Sci.* **2008**, *254*, 6436–6440.
- (20) Jiang, T.; Lough, A. J.; Ozin, G. A.; Young, D.; Bedard, R. L. *Chem. Mater.* **1995**, *7*, 245–248.
- (21) Boonsalee, S.; Gudavarthy, R. V.; Bohannan, E. W.; Switzer, J. A. *Chem. Mater.* **2008**, *20*, 5737–5742.
- (22) Zhang, Y.; Lu, J.; Shen, S.; Xu, H.; Wang, Q. *Chem. Commun.* **2011**, *47*, 5226–5228.
- (23) Zhu, H.; Yang, D.; Zhang, H. *Mater. Lett.* **2006**, *60*, 2686–2689.
- (24) Zhang, H.; Hu, C.; Wang, X.; Xi, Y.; Li, X. *J. Alloys Compd.* **2012**, *513*, 1–5.
- (25) Hong, S. Y.; Popovitz-Biro, R.; Prior, Y.; Tenne, R. *J. Am. Chem. Soc.* **2003**, *125*, 10470–10474.
- (26) Greyson, E. C.; Barton, J. E.; Odom, T. W. *Small* **2006**, *2*, 368–371.
- (27) Reddy, K. R.; Reddy, N. K.; Miles, R. *Sol. Energy Mater. Sol. Cells* **2006**, *90*, 3041–3046.
- (28) Noguchi, H.; Setiyadi, A.; Tanamura, H.; Nagatomo, T.; Omoto, O. *Sol. Energy Mater. Sol. Cells* **1994**, *35*, 325–331.
- (29) Sugiyama, M.; Murata, Y.; Shimizu, T.; Ramya, K.; Venkataiah, C.; Sato, T.; Reddy, K. T. R. *Jpn. J. Appl. Phys.* **2011**, *50*, 05FH03.
- (30) Parenteau, M.; Carlone, C. *Phys. Rev. B* **1990**, *41*, 5227–5234.
- (31) Vidal, J.; Lany, S.; d’Avezac, M.; Zunger, A.; Zakutayev, A.; Francis, J.; Tate, J. *Appl. Phys. Lett.* **2012**, *100*, 032104.
- (32) Shockley, W.; Queisser, H. J. *J. Appl. Phys.* **1961**, *32*, 510–&.
- (33) Ferekides, C. S.; Balasubramanian, U.; Mamazza, R.; Viswanathan, V.; Zhao, H.; Morel, D. L. *Sol. Energy* **2004**, *77*, 823–830.
- (34) Albers, W.; Haas, C.; Vink, H. J.; Wasscher, J. D. *J. Appl. Phys.* **1961**, *32*, 2220.
- (35) Hohenberg, P.; Kohn, W. *Phys. Rev.* **1964**, *136*, B864–B871.
- (36) Kohn, W.; Sham, L. J. *Phys. Rev.* **1965**, *140*, A1133–A1138.
- (37) Havu, V.; Blum, V.; Havu, P.; Scheffler, M. *J. Comput. Phys.* **2009**, *228*, 8367–8379.
- (38) Perdew, J. P.; Ruzsinszky, A.; Csonka, G. I.; Vydrov, O. A.; Scuseria, G. E.; Constantin, L. A.; Zhou, X.; Burke, K. *Phys. Rev. Lett.* **2008**, *100*, 136406.
- (39) van Lenthe, E.; Baerends, E. J.; Snijders, J. G. *J. Chem. Phys.* **1994**, *101*, 9783–9792.
- (40) Head, J. D.; Zerner, M. C. *Chem. Phys. Lett.* **1985**, *122*, 264–270.
- (41) Payne, D. J.; Egdell, R. G.; Walsh, A.; Watson, G. W.; Guo, J.; Glans, P.-A.; Learmonth, T.; Smith, K. E. *Phys. Rev. Lett.* **2006**, *96*, 157403.
- (42) Mariano, A. N.; Chopra, K. L. *Appl. Phys. Lett.* **1967**, *10*, 282–284.
- (43) Chattopadhyay, T.; Pannetier, J.; Von Schnering, H. G. *J. Phys. Chem. Solids* **1986**, *47*, 879–885.
- (44) Badachhape, S.; Goswami, A. *J. Phys. Soc. Jpn.* **1962**, *17*, 251–253.
- (45) Bilenkii, B.; Mikolaichuk, A.; Freik, D. *Phys. Status Solidi* **1968**, *28*, K5–K7.
- (46) Arora, S. K.; Patel, D. H.; Agarwal, M. K. *Cryst. Res. Technol.* **1993**, *28*, 623–627.
- (47) Moore, W. J.; Pauling, L. *J. Am. Chem. Soc.* **1941**, *63*, 1392–1394.
- (48) Baur, W. H.; Khan, A. A. *Acta Crystallogr., Sect. B: Struct. Sci.* **1971**, *27*, 2133–2139.
- (49) Wiedemeier, H.; Csillag, F. J. *Z. Kristallogr.* **1979**, *149*, 17.
- (50) Kresse, G.; Furthmüller, J. *Phys. Rev. B* **1996**, *54*, 11169–11186.
- (51) Scragg, J. J.; Dale, P. J.; Colombara, D.; Peter, L. M. *ChemPhysChem* **2012**, *13*, 3035–3046.
- (52) *CRC Handbook of Chemistry and Physics*, 92nd ed.; CRC Press: Boca Raton, FL, 2011–2012.
- (53) Sharma, R.; Chang, Y. *J. Phase Equilib.* **1986**, *7*, 269–273.
- (54) Novoselova, A. V.; Zlomanov, V. P.; Karbanov, S. G.; Matveyev, O. V.; Gas’kov, A. M. *Prog. Solid State Chem.* **1972**, *7*, 85–115.
- (55) Piacente, V.; Foglia, S.; Scardala, P. *ChemInform* **1992**, *23*.
- (56) Tanůševski, A.; Poelman, D. *Sol. Energy Mater. Sol. Cells* **2003**, *80*, 297–303.
- (57) Burton, L. A.; Walsh, A. *J. Solid State Chem.* **2012**, *196*, 157–160.
- (58) Stoltzfus, M. W.; Woodward, P. M.; Seshadri, R.; Klepeis, J.-H.; Bursten, B. *Inorg. Chem.* **2007**, *46*, 3839–3850.
- (59) Walsh, A.; Watson, G. W. *J. Phys. Chem. B* **2005**, *109*, 18868–18875.
- (60) Lefebvre, I.; Szymanski, M. A.; Olivier-Fourcade, J.; Jumas, J. C. *Phys. Rev. B* **1998**, *58*, 1896–1906.
- (61) Scanlon, D. O.; Walsh, A. *Appl. Phys. Lett.* **2012**, *100*, 251911.
- (62) Momma, K.; Izumi, F. *J. Appl. Crystallogr.* **2011**, *44*, 1272–1276.